

A Flexible Nanocrystal Photovoltaic Ultraviolet Photodetector on a Plant Membrane

Jingda Wu and Lih Y. Lin*

Ultraviolet (UV) detection has been extensively studied thanks to its wide applications in communication, pollution monitoring, and medicine. While high-performance UV photodetection has been achieved in previous research work^[1–8] and even for commercial use, the rigidity of these devices limits their usage for applications requiring portability and wearability, which is the current trend for commercial electronics. This is where solution-processable nanomaterials can make distinguishable contributions. Low-cost flexible devices have been made possible by utilizing materials such as nanocrystal (NC) quantum dots and nanorods. Wet-chemistry synthesis^[9–11] of these materials not only helps reduce the material cost, but also offers solution-processability, which enables low-cost, facile, and large-scale fabrication. In addition, the 3D confinement of electrons in NCs leads to high-quantum efficiency and a tunable bandgap depending on the particle size,^[12,13] and thus offering the convenience of tuning the absorption spectrum edge for different optoelectronic applications. In terms of UV detection, ZnO NC is a very promising material for flexible devices. With a bulk bandgap of 3.37 eV, ZnO has excellent absorption in UV and remains transparent to visible light, i.e., it is a naturally visible-blind material. Its large exciton binding energy (60 meV) also suggests that it is a good candidate for high-performance optoelectronic devices. Due to the above-mentioned advantages, a great variety of high-performance ZnO-based UV detectors^[2–4,14–19] have been demonstrated in the literature, which further proves the feasibility of applying them towards UV detection applications.

Substrate choice is important for flexible devices. Recently, cellulose structures have attracted much research interest for flexible optoelectronic devices and have been used in photodetectors,^[20] photovoltaics,^[21,22] light emitting devices and displays.^[23–25] Unlike polyethylene terephthalate (PET) or thin film glass which are conventional materials for flexible substrates that have been dominantly used in the industry, cellulose structure is much more environmental friendly and abundant in nature, which also helps lower the material cost. While paper is the most widely used cellulose structure, its high porosity^[20] affects the quality of the films deposited on the substrate. Hence researchers have been developing new synthesis methods and using nanofibrous structures^[26–28] for smoother and also more transparent papers. Nevertheless, we discovered

that the porosity of paper could be turned into advantages when its utilization in the device fabrication is optimized. The large surface-volume ratio of porous structures facilitates the adhesion of NCs and thus eases the material deposition. The porosity also enhances light scattering (large optical haze^[26]) and increases the light absorption of the active material, which improves the overall device performance. Furthermore, paper is able to act as a good interspacing layer to prevent short-circuit problem commonly encountered in fabricating vertical devices with NCs on flexible substrates. People have long used paper as a dielectric layer for energy storage devices^[29,30] and field effect transistors.^[25,31] Based on these rationales, we have fabricated CdSe quantum dot photodetectors on tracing papers and achieved consistent results,^[32] yet the large thickness of conventional papers deteriorates the carrier transportation and reduces the optical transparency as well. The high density of fibers in a paper also reduces the concentration of quantum dots that can be incorporated into the structure, which further reduces the device performance.

On the other hand, Mother Nature has supplied us with a variety of thin and porous cellulose structures with good transparency in the form of plant membranes, such as reed inner fibrous structures or leaf-structuring membranes. In this communication, UV photodetectors are fabricated, as far as we know, for the first time on a reed plant membrane (**Figure 1a**). The material is commercially available as the vibration membrane for Chinese bamboo flutes. At a thickness of $\approx 5 \mu\text{m}$ when compressed, the membrane is significantly thinner than most of the commercial papers ($>30 \mu\text{m}$) and offers much better transparency. We designed a vertical structure for the device that consists of a ZnO NC-embedded reed membrane sandwiched between gold and aluminum electrodes, as shown in **Figure 1b**. Though lateral photoconductor structure is typically of interest due to its simplicity and potentially high optical gain, ZnO NC-based flexible UV photoconductors in general suffer from slow response^[15–18,33–35] due to the large number of trapping states and slow carrier mobilities compared to bulk semiconductor material. By using the cellulose structure as an interspacing layer with the active material embedded, a Schottky junction structure can be readily achieved between ZnO and Au as shown in **Figure 1c**, which improves the response speed. While thin-film Au and indium tin oxide (ITO) can both serve as transparent electrodes and have high work functions that can result in Schottky junctions interfacing with ZnO, ITO becomes opaque at UV region and it also has poor flexibility due to the ceramic-like crystal structure. Given these plus further consideration in fabrication simplicity, we chose Au as the transparent electrode for our device despite that ITO is currently the most widely used transparent electrode material. Furthermore, Au also shows good adhesion on the cellulose

J. Wu, Prof. L. Y. Lin
Electrical Engineering Department
University of Washington
185 Stevens Way, Seattle, WA 98195, USA
E-mail: lylin@uw.edu

DOI: 10.1002/adom.201500198



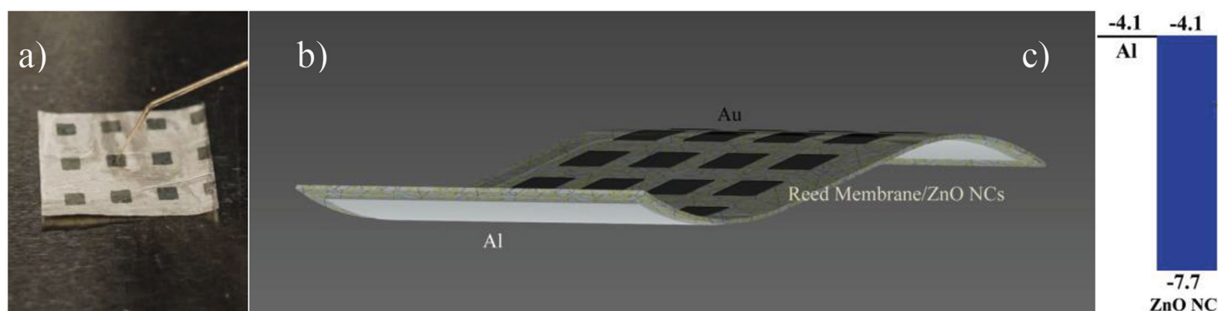


Figure 1. a) An array of ZnO UV flexible photodetectors fabricated on a reed membrane. The photograph shows one of them under test using a probe; b) Schematics of the device structure; c) The energy band diagram of the device (unit: eV).

structure and requires no additional adhesion layer, which further simplifies the deposition process and increases the transparency and conductivity of the device as well. An Ohmic contact is formed between Al and ZnO (Figure 1c). With such a device design, we are able to operate the device without external bias, i.e., the device can be operated with photovoltaic effect and is therefore self-powered. At zero bias, the device achieved an overall external quantum efficiency (EQE) of >1% throughout the UV region and peaked at >3% at 350 nm wavelength. The response speed was characterized to be less than 1 s. The performance is comparable to, if not better than, most of the flexible^[14,16–18,33] or even rigid UV detectors,^[1,3–5,19] in the literature. A performance comparison between devices on tracing papers and reed membranes is also made. The device fabricated on the tracing paper performs more like a photoconductor, little or no photoresponse is observed at zero bias and the device also shows lower EQE under bias.

ZnO NCs are prepared using the well-developed synthesis method^[9] by heating up zinc acetate dihydrate ($\text{Zn}(\text{Ac})_2 \cdot 2\text{H}_2\text{O}$) alcoholic solution under a basic ($\text{pH} > 7$) environment. A particle size of 6–8 nm is achieved with little influence from the variation of temperature (60 °C–65 °C) during synthesis. ZnO NCs are embedded into the cellulose structure through a facile soaking process. However, natural bio-membranes have cells tightly bind together to enforce the mechanical strength of the structure, thus leaving little room for penetration of external objects, which are ZnO NCs in this case. To solve this issue, we treat the membranes in KOH solution first before ZnO deposition to dissolve the proteins and leave with just the cellulose structure to open up more room for NC attachment. **Figure 2** shows SEM images of the bio-cellulose structures before and after ZnO NC deposition. We can see that the NCs formed a smooth and continuous layer embedded in the cellulose structure. A visual optical transparency comparison between a reed membrane and a tracing paper before and after ZnO deposition is presented in **Figure 3a,b**. The reed membrane is more transparent, with $\approx 85\%$ visible light transmission, than the tracing paper ($\approx 65\%$), as shown clearly in **Figure 3a**. Very high optical haze is also observed for both materials (**Figure 3b**), which confirms enhanced light scattering and the potential for using cellulose materials for optoelectronic applications involving light absorption. But what is surprising is that the reed membrane becomes more transparent visually after the embedment of ZnO NCs, as more details of the background

image are preserved. This can be possibly attributed to the waveguiding effect of ZnO. ZnO has a slightly larger refractive index ($n \approx 2$) compared to the cellulose ($n \approx 1.47$), and thus scattering is possibly reduced in the spacing between the cellulose fibers and more light is transmitted through channels formed by ZnO NCs. A similar effect is also observed in the tracing paper, but not as significant as that in the reed membrane, due to the thicker structure. To confirm the above observation and better understand how ZnO influences the amount of light transmitting through the substrates, especially at the UV range, we measured the light transmittance (T) before and after ZnO embedment and show the corresponding transmittance ratio ($T_{\text{after}}/T_{\text{before}}$) versus illumination wavelength in **Figure 3c** for both the reed membrane and the tracing paper. Note that **Figure 3c** is generated from UV–vis transmittance data, which depends on the distance between the photodetector and the membrane due to the large optical haze. Therefore the results may not directly reflect the actual transmittance, but it well reflects the phenomena we observe. We clearly saw enhanced transmission of light at visible range. At UV range, the transmittance is significantly reduced for both materials after ZnO NCs are embedded due to the absorption of ZnO NCs, which contributes to UV photodetection.

Au thin films of 25 nm thickness with a square pattern size of $1.8 \times 1.8 \text{ mm}^2$ defined by a shadow mask are thermally evaporated onto the ZnO-embedded reed membrane. At such a thickness, the gold layer appears to be of transparent dark green (**Figure 1a**) instead of opaque gold. An Al film of 150 nm is also thermally evaporated on the other side of the reed membrane to serve as the back common contact pad. The current–voltage response of the device is measured under different intensities at 365 nm UV light illumination and the results are shown in **Figure 4a**. The I – V curves show Schottky junction behavior. The dependence of the current I on the applied bias V can be expressed by elsewhere.^[36]

$$I = I_s [\exp(qV / \eta kT) - 1] \quad (1)$$

where I_s is the reverse-bias saturation current, q is the net charge of an electron ($1.6 \times 10^{-19} \text{ C}$), k is the Boltzmann constant ($1.38 \times 10^{-23} \text{ m}^2 \text{ kg s}^{-2} \text{ K}^{-1}$), η is the ideality factor of the device, and T is the absolute temperature, which is room temperature (300 K) for the experiments. Through curve-fitting the dark response, we obtained a saturation current I_s of $1.29 \times 10^{-9} \text{ A}$

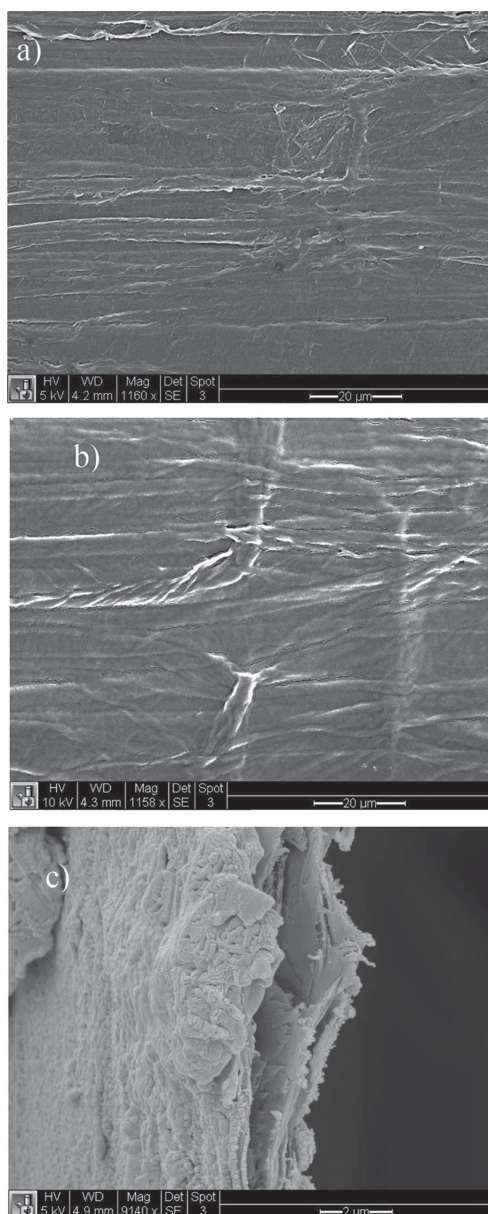


Figure 2. SEM images of the bio-cellulose structure a) before, and b) after ZnO NC deposition; c) a cross-sectional view of how ZnO NCs wrap around the cellulose structure.

and an ideality factor η of 7.95. While the ideality factor of an ideal Schottky diode ranges from 1 to 2 depending on whether the diffusion current or the recombination current is dominant, our particularly large ideality factor indicates that more mechanisms influence the performance of the device. It is known that crystal defect states and metal-semiconductor interface contamination will lead to large η .^[37] ZnO in NC forms are typically prone to having many surface states,^[38] which greatly influence the optoelectronic properties of the material due to the large surface-to-volume ratio of nanosized particles. The greenish yellow fluorescence of ZnO NCs under 365 nm UV excitation (Figure 4a, inset) indicates that there are deep level defects in the material. Such large η has also been found

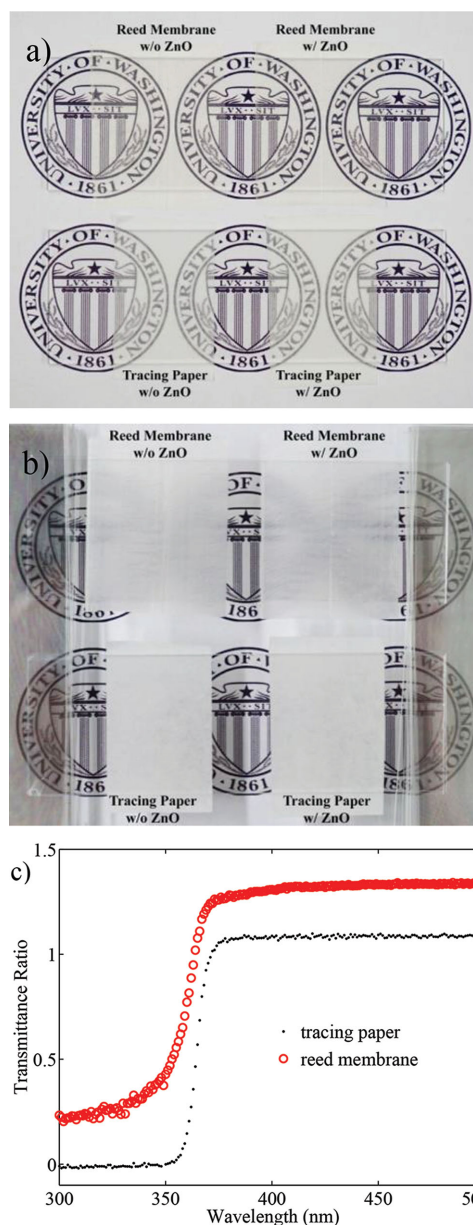


Figure 3. a,b) Visual optical transparency comparison between reed membranes and tracing papers, before and after ZnO NC deposition. A glass slide is placed on top of the materials for fixation purpose. The materials are placed a) close to, and b) away from the background image. c) The optical transmission comparison between the two cellulose materials over UV-vis range. The data show the ratio of transmittance after ZnO NC deposition to that before the deposition. The transmittance is enhanced in visible wavelengths by the ZnO NCs, but reduced at UV wavelengths due to ZnO absorption as expected.

from other works in the literature^[39,40] that utilize NCs or other nanostructures, even on rigid substrates. The saturation current can be written as

$$I_s = A_{\text{eff}} A^* T^2 \exp(q\Phi_B/kT) \quad (2)$$

where A^* is the Richardson constant ($32 \text{ A cm}^{-2} \text{ K}^{-2}$ for ZnO), A_{eff} is the effective device area for illumination, $q\Phi_B$ is the

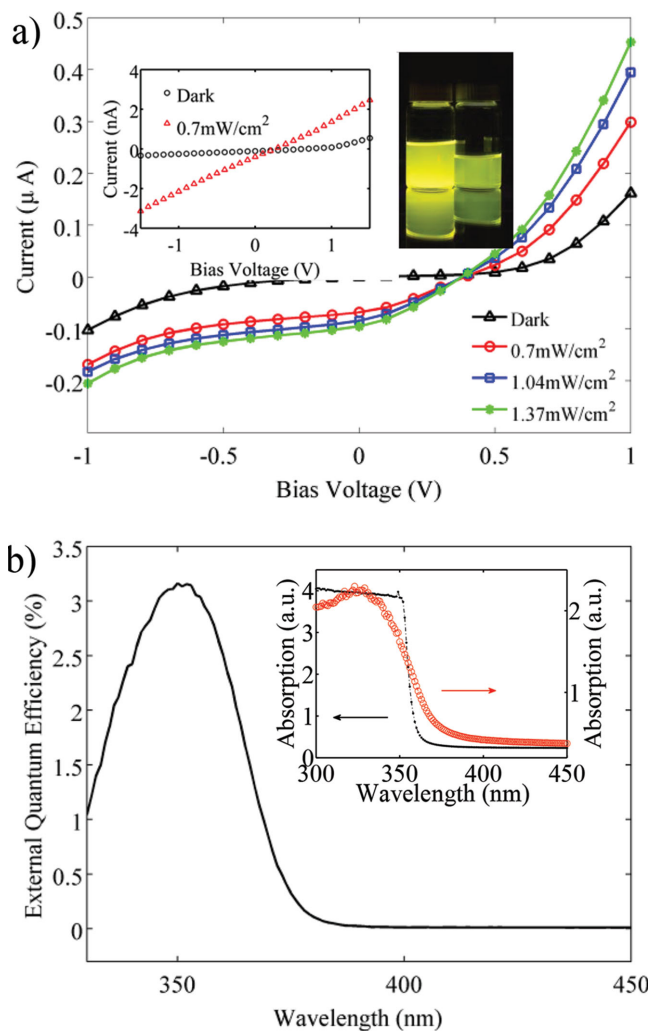


Figure 4. a) Current–voltage characteristics of the UV flexible photodetector on reed membrane under 365 nm light illumination at different intensities. The left inset figure shows performance from a similar device fabricated on the tracing paper. The right inset shows the fluorescence from two bottles of ZnO NCs under 365 nm light excitation. b) EQE curve of the device (inset: ZnO NC absorption spectra; the black and red curves correspond to ZnO NC in solution and on reed membrane, respectively).

Schottky barrier height, which is fitted to be 0.83 eV for our device. While it is commonly known that larger n corresponds to lower barrier height due to charge accumulation in the defect states,^[37] the noticeably large barrier height of our device may be due to the non-ideality of the device and cellulose's insulating nature.

From the photoresponses shown in Figure 4a when under UV illumination, we observed photovoltaic responses, with an open-circuit voltage of ≈ 0.4 V, where all the curves intercept. For energy-saving purpose, it is preferable to operate the device under zero bias. The photoresponsivities of the device under light intensities of 0.7, 1.04, and 1.37 mW cm^{-2} at zero bias are 3.7, 3, and 2.5 mA W^{-1} , which corresponds to EQEs of 1.08%, 0.87%, and 0.75%, respectively, at 365 nm wavelength. The slightly decreasing performance at higher intensities is due to the device saturation under more intense light illumination.

The I - V curves of a device fabricated on a tracing paper using the same method measured under 365 nm UV illumination of 0.7 mW cm^{-2} intensity is also shown in the inset of Figure 4a for comparison. Despite better conductance of the gold film, it appears to have much lower photoresponsivity performance with more photoconductor-like characteristics, mostly due to the thick and dense cellulose structure. The spectral-wise EQE measurement result of the device on reed membrane is shown in Figure 4b. The device performance peaks at ≈ 350 nm with EQEs over 3%, which corresponds to photoresponsivities of >8.5 mA W^{-1} . The photoresponse cuts off gradually at ≈ 375 nm, which corresponds well with the bandgap of bulk ZnO. However, the absorption curve of ZnO NCs in solution form (inset of Figure 4b, black curve) shows a sharp cut off at ≈ 360 nm and flatter UV absorption, which is understandably due to quantum size confinement. The discrepancy may be due to the agglomeration of the ZnO NCs when deposited on the reed membrane, which results in a more bulk-like energy bandgap structure. To verify this, we performed absorption measurement of ZnO NCs on reed membrane, and the result is shown as the red curve in the inset of Figure 4b, which exhibits a trend similar to the EQE curve. The blue shift of the peak is due to the absorption of the reed membrane, which accounts for the decreasing performance of the photodetector at deeper UV range. No response is observed at visible range, which indicates that this device functions as a naturally visible-blind UV detector.

Another important factor that limits the usage of current flexible ZnO UV detectors is the response speed. Most of these devices are made of photoconductive structure, which are typically of low speed due to slow carrier recombination. In addition, the oxygen molecule adsorption and desorption processes^[41–43] in ZnO materials, especially for NCs, further reduce the response speed. In dark, oxygen molecules are adsorbed by ZnO NC and combined with free electrons on the surface [$\text{O}_2(\text{g}) + \text{e}^- \rightarrow \text{O}_2^-(\text{ad})$]. When free electron-hole pairs are generated upon UV light illumination in ZnO NC photoconductors, holes are trapped by the oxygen surface states [$\text{O}_2^-(\text{ad}) + \text{h}^+ \rightarrow \text{O}_2(\text{g})$] and leave free electrons circulating the circuit before re-adsorbed by the oxygen molecules or recombine with holes. Due to the involvement of oxygen molecule in the process, it takes longer time to reach equilibrium and thus slows down the response speed. However, in Schottky junctions charge carriers are quickly extracted by the built-in potential in the narrow depletion region upon excitation at zero bias. Hence Schottky junction devices in general have much faster response speed, as demonstrated by our device (Figure 5). Sub-second response times are observed for both rise and fall curves. Though the oxygen adsorption and desorption processes also play a role in Schottky devices by influencing the barrier height of the junction, which also increased the non-ideality of the diode, their impact on the response time is not as significant as that in a photoconductor. But we do see a slower decay rate than the rise rate, which may be due to these processes.

Table 1 shows the device performance comparison among various UV photodetectors reported in literature and this work. Both flexible devices and rigid devices with photodiode structures are included. Our device shows faster time response than most of these flexible devices with photoconductor structures and at the same time offers comparable performance to some

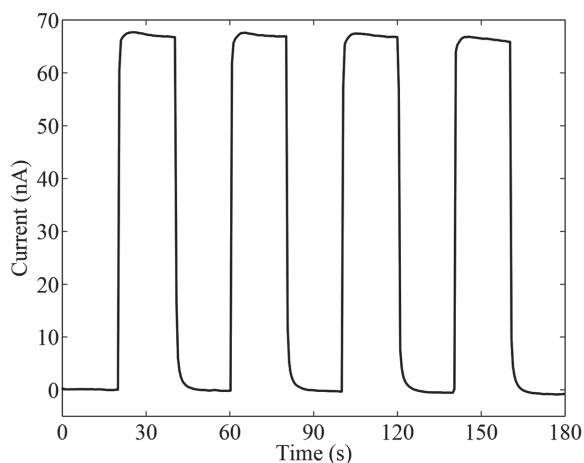


Figure 5. Time-response of the ZnO nanocrystal UV detector on cellulose structure.

of the work in photoresponsivity under zero bias. While some of these flexible devices could achieve better photoresponsivities, their fabrication methods are more complicated and some involves the assistance of other materials. Much higher bias voltage is often required to achieve high photoresponsivities for these devices. Compared to rigid p–n or Schottky junction-based devices, the photoresponsivity is comparable while the response speed is understandably slower due to the structure and thickness of the cellulose material. Overall, our device balances the response speed with photoresponsivity, while at the same time offers flexibility with a simple fabrication process.

Being a flexible device, the UV detector performance should not degrade due to bending. The device performance under different numbers of bending cycles is measured and the results are shown in **Figure 6a**. Measurements are taken after

0, 40, 80, and 160 bends around a pen with a radius of 4 mm (Figure 6 inset) under an illumination intensity of $65 \mu\text{W cm}^{-2}$ at 365 nm wavelength. The photocurrent over 10 s time period after each bending is plot in the figure. A slight performance increase is observed after each bending. Since the device was tested without rest after bending, it is possible that the cellulose structure was under compression, which squeezed the NCs and facilitates the carriers to tunnel through nearby NCs, and thus improved the overall conductivity of the ZnO NC film. To further understand the effect of bending on the device performance, we tested a device under different bending radii, and the results are shown in Figure 6b. The photocurrents over 80 s time period at bending radii of infinity (flat condition), 10, 9, 7, and 6 mm (over a stainless-steel object (Figure 6b inset)) under an illumination intensity of $76 \mu\text{W cm}^{-2}$ at 365 nm wavelength are plot in the figure. The increased noise shown in the figure is more likely due to the bending test system instead of the device itself due to the non-ideal back contact. Overall, slight photocurrent increase was observed at smaller bending radii, which is in accordance with the previous bending cycle test results.

In conclusion, our work demonstrates the potential of natural bio-cellulose structures for fabricating flexible optoelectronic devices. To the best of our knowledge, this is the first time that flexible UV photodetectors are built on a natural reed membrane with ZnO NCs embedded. The Schottky junction structure enables the device to function as a self-powered device and responds at a much faster speed than most of the metal oxide-based flexible photoconductive detectors. An EQE over 3%, corresponding to a photoresponsivity of $>8.5 \text{ mA W}^{-1}$, has been achieved under zero bias at 350 nm, which is comparable to some of the rigid devices with photodiode structures, thanks to the thin and porous structure of the reed membrane. Though commercial papers can also be used to make flexible photodetectors using a similar method, the dense and thick

Table 1. Comparison between UV detectors in the literature.

Material ^{a)}	Structure (PC/PD) ^{b)}	Flexible (Y/N)	Rise/fall time ^{c)} [s]	Photoresponsivity ^{d)} [mA W^{-1}]	Bias voltage [V]	Wavelength ^{e)} [nm]	Refs.
ZnS–ZnO	PC	Y	0.77/0.73	<1	10	320	[14]
ZnO NW	PC	Y	>400	>1 A W^{-1}	3	–	[15]
ZnO–rGO	PC	Y	6/3.5	<<1	10	365	[16]
TiO ₂	PC	Y	1.4/6.1	16	1	345	[33]
SnO ₂	PC	Y	>20/>50	230	5	320	[34]
ZnO NW	PC	Y	19.6/2.5	8.3	0.5	365	[17]
ZnO–Au NP	PC	Y	≈40/>56	1.51×10^5	50	350	[18]
TiO ₂	PD	N	0.15/0.05	25	0	350	[1]
ZnO/p-Si	PD	N	<0.3	408	0	355	[2]
ZnO-organic	PD	N	0.2 ms/0.95 ms	0.017	0	390	[19]
ZnO NW	PD	N	81 ms	1.82	0	365	[3]
ZnO NR–CuSCN	PD	N	0.5 μs /6.7 μs	7.5	0	355	[4]
Organic	PD	N	20 ns/888 ns	22.5	0	350	[5]
ZnO NC	PD	Y	≈0.5/≈1	>8.5	0	350	This work

^{a)}NW stands for nanowire, NR for nanorod and rGO for reduced graphene oxide; ^{b)}PC stands for photoconductor, and PD stands for photodiode; ^{c)}Different work might use different models for response time calculation based on experimental data; ^{d)}Some of the results are calculated based on the given information from the reference; ^{e)}Wavelength resulting in the maximum photoresponsivity.

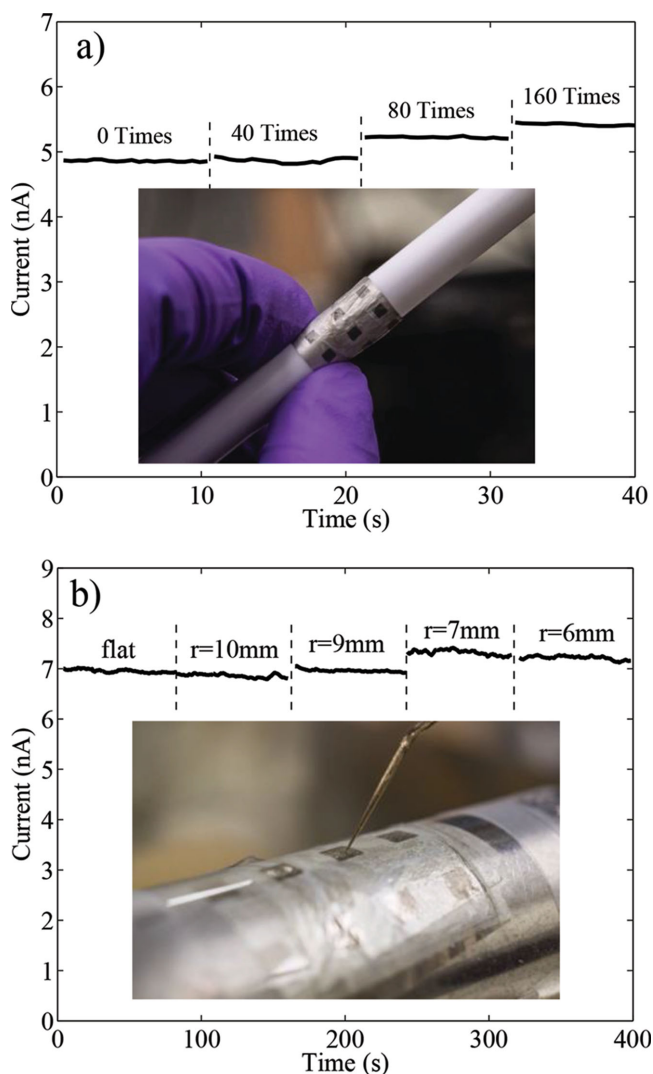


Figure 6. The device performance in photocurrent a) measured for a duration of 10 s after different times of continuous bending (inset: photograph of the device bent around a pen with a radius of 4 mm); b) after bending at different radii (inset: photograph of the device under test on a cylindrical stainless-steel object).

cellulose structure can reduce the performance of the device. While this work focuses on photodetection, ZnO NC is also an excellent material for room-temperature gas sensing that involves the oxygen molecule adsorption and desorption processes, thanks to its large surface-to-volume ratio. Potential use of ZnO NCs for sensing gases such as hydrogen, nitric oxide, or ethanol has been reported,^[44–47] and our integration with porous flexible cellulose structures offers the advantages of light weight, wearability, and portability without sacrificing sensitivity.

Experimental Section

ZnO Nanocrystal Synthesis: ZnO NCs were synthesized using a well-developed wet-chemistry method. Zinc acetate dihydrate (2.92 g) was dissolved in methanol (125 mL), and potassium hydroxide (KOH)

(1.48 g) was dissolved in methanol (65 mL) upon sonication and then mixed with Zn(Ac)₂·2H₂O solutions drop-wise at ≈65 °C. The reaction then took two and a half hours with the solution turning turbid and followed by centrifuging to precipitate out the NCs. The precipitation was washed in methanol twice with centrifuging and then dissolved in 15 mL butanol and 1 mL chloroform to form a clear and transparent solution with a ZnO NC concentration of ≈30 mg mL⁻¹. A NC size of ≈6 nm was achieved through this process. These NCs were air-stable for weeks with continuous magnetic stirring.

Device Fabrication: Before depositing ZnO NCs, reed membranes were soaked in KOH overnight and then rinsed in methanol and isopropanol. After that, they were soaked in ZnO NC solution overnight and had the NCs embedded in the cellulose structure. Upon being dried in vacuum, Al films with a thickness of 150 nm were thermally evaporated on one side of these substrates to form common contact, and followed by another thermal evaporation of 25 nm gold film with features of 1.8 mm × 1.8 mm defined by shadow masks to work as transparent electrodes. The deposition rate played an important role for Au. Slow deposition introduced isolated Au islands and reduced the conductivity of Au film significantly, thus deteriorated the device performance. A rate higher than 1 Å s⁻¹ was preferred in our case.

Device and Material Characterization: I–V responses and EQEs were measured with a Keithley 6430 sub-femtoamp sourcemeter through NI LabView software control. A tungsten light source was used to illuminate the device through an Acton Research SpectraPro 275 monochromator to provide wavelength selectivity for the EQE measurement. A 365 nm UV LED was used for the I–V measurement. The SEM images were obtained by a Sirion SEM in the Nanotech User Facility at the University of Washington. UV–vis absorption and transmission spectra were measured with Varian Cary 5000 UV–vis–NIR Spectrophotometer. All measurements were performed at room temperature (300 K).

Acknowledgement

The authors thank Long Gui at the University of Washington for the help on nanoparticle size characterization. The authors also thank Mike Carroll at the University of Washington for helpful discussions on EQE measurement. Part of the work is performed at the Nanotech User Facility (NTUF) and Photonics Research Center (PRC) at the University of Washington.

Received: April 15, 2015

Revised: May 18, 2015

Published online: June 23, 2015

- [1] Y. Xie, L. Wei, G. Wei, Q. Li, D. Wang, Y. Chen, S. Yan, G. Liu, L. Mei, J. Jiao, *Nanoscale Res. Lett.* **2013**, *8*, 1.
- [2] J. Qi, X. Hu, Z. Wang, X. Li, W. Liu, Y. Zhang, *Nanoscale* **2014**, *6*, 6025.
- [3] Z. Bai, X. Chen, X. Yan, X. Zheng, Z. Kang, Y. Zhang, *Phys. Chem. Chem. Phys.* **2014**, *16*, 9525.
- [4] S. M. Hatch, J. Briscoe, S. Dunn, *Adv. Mater.* **2013**, *25*, 867.
- [5] H. L. Zhu, W. C. H. Choy, W. E. I. Sha, X. Ren, *Adv. Optical Mater.* **2014**, *2*, 1082.
- [6] X. Fang, L. Hu, K. Huo, B. Gao, L. Zhao, M. Liao, P. K. Chu, Y. Bando, D. Golberg, *Adv. Funct. Mater.* **2011**, *21*, 3907.
- [7] L. Hu, J. Yan, M. Liao, H. Xiang, X. Gong, L. Zhang, X. Fang, *Adv. Mater.* **2012**, *24*, 2305.
- [8] H. Liu, Z. Zhang, L. Hu, N. Gao, L. Sang, M. Liao, R. Ma, F. Xu, X. Fang, *Adv. Optical Mater.* **2014**, *2*, 771.
- [9] C. Pacholski, A. Kornowski, H. Weller, *Angew. Chem. Int. Ed.* **2002**, *41*, 1188.
- [10] X. Wang, J. Zhuang, Q. Peng, Y. Li, *Nature* **2005**, *437*, 121.

- [11] D. Liu, T. L. Kelly, *Nat. Photonics* **2013**, *8*, 133.
- [12] R. Viswanatha, S. Sapra, B. Satpati, P. V. Satyam, B. N. Dev, D. D. Sarma, *J. Mater. Chem.* **2004**, *14*, 661.
- [13] D. V. Talapin, J.-S. Lee, M. V. Kovalenko, E. V. Shevchenko, *Chem. Rev.* **2010**, *110*, 389.
- [14] W. Tian, C. Zhang, T. Zhai, S.-L. Li, X. Wang, J. Liu, X. Jie, D. Liu, M. Liao, Y. Koide, D. Golberg, Y. Bando, *Adv. Mater.* **2014**, *26*, 3088.
- [15] S. Bai, W. Wu, Y. Qin, N. Cui, D. J. Bayerl, X. Wang, *Adv. Funct. Mater.* **2011**, *21*, 4464.
- [16] Z. Wang, X. Zhan, Y. Wang, S. Muhammad, Y. Huang, J. He, *Nanoscale* **2012**, *4*, 2678.
- [17] L. Ren, T. Tian, Y. Li, J. Huang, X. Zhao, *ACS Appl. Mater. Interfaces* **2013**, *5*, 5861.
- [18] Z. Jin, L. Gao, Q. Zhou, J. Wang, *Sci. Rep.* **2014**, *4*, 4268.
- [19] O. Game, U. Singh, T. Kumari, A. Banpurkar, S. Ogale, *Nanoscale* **2014**, *6*, 503.
- [20] A. Manekthodi, M.-Y. Lu, C. W. Wang, L.-J. Chen, *Adv. Mater.* **2010**, *22*, 4059.
- [21] Y. Zhou, C. Fuentes-Hernandez, T. M. Khan, J. C. Liu, J. Hsu, J. W. Shim, A. Dindar, J. P. Youngblood, R. J. Moon, B. Kippelen, *Sci. Rep.* **2013**, *3*, 1536.
- [22] M. C. Barr, J. A. Rowehl, R. R. Lunt, J. Xu, A. Wang, C. M. Boyce, S. G. Im, V. Bulovic, K. K. Gleason, *Adv. Mater.* **2011**, *23*, 3499.
- [23] H. Zhu, Z. Xiao, D. Liu, Y. Li, N. J. Weadock, Z. Fang, J. Huang, L. Hu, *Energy Environ. Sci.* **2013**, *6*, 2105.
- [24] Y. Okahisa, A. Yoshida, S. Miyaguchi, H. Yano, *Compos. Sci. Technol.* **2009**, *69*, 1958.
- [25] P. Andersson, D. Nilsson, P. O. Svensson, M. Chen, A. Malmström, T. Remonen, T. Kugler, M. Berggren, *Adv. Mater.* **2002**, *14*, 1460.
- [26] Z. Fang, H. Zhu, Y. Yuan, D. Ha, S. Zhu, C. Preston, Q. Chen, Y. Li, X. Han, S. Lee, G. Chen, T. Li, J. Munday, J. Huang, L. Hu, *Nano Lett.* **2014**, *14*, 765.
- [27] Z. Shi, G. O. Phillips, G. Yang, *Nanoscale* **2013**, *5*, 3194.
- [28] H. Zhu, Z. Fang, C. Preston, Y. Li, L. Hu, *Energy Environ. Sci.* **2014**, *7*, 269.
- [29] V. Wood, M. J. Panzer, J. Chen, M. S. Bradley, J. E. Halpert, M. G. Bawendi, V. Bulović, *Adv. Mater.* **2009**, *21*, 2151.
- [30] H. Zhu, Z. Jia, Y. Chen, N. Weadock, J. Wan, O. Vaaland, X. Han, T. Li, L. Hu, *Nano Lett.* **2013**, *13*, 3093.
- [31] E. Fortunato, N. Correia, P. Barquinha, L. Pereira, G. Goncalves, R. Martins, *IEEE Electron Device Lett.* **2008**, *29*, 988.
- [32] J. Wu, L. Y. Lin, *IEEE Photonics Technol. Lett.* **2014**, *26*, 737.
- [33] Z. Wang, H. Wang, B. Liu, W. Qiu, J. Zhang, S. Ran, H. Huang, J. Xu, H. Han, D. Chen, G. Shen, *ACS Nano* **2011**, *5*, 8412.
- [34] W. Tian, C. Zhang, T. Zhai, S.-L. Li, X. Wang, M. Liao, K. Tsukagoshi, D. Golberg, Y. Bando, *Chem. Commun.* **2013**, *49*, 3739.
- [35] K. ul Hasan, O. Nur, M. Willander, *Appl. Phys. Lett.* **2012**, *100*, 211104.
- [36] S. M. Sze, K. K. Ng, *Physics of Semiconductor Devices*, John Wiley & Sons, Inc., Hoboken, NJ, USA **2007**.
- [37] L. J. Brillson, Y. Lu, *J. Appl. Phys.* **2011**, *109*, 121301.
- [38] N. S. Norberg, D. R. Gamelin, *J. Phys. Chem. B* **2005**, *109*, 20810.
- [39] M. C. Newton, S. Firth, P. A. Warburton, *Appl. Phys. Lett.* **2006**, *89*, 072104.
- [40] Z. Yuan, *Phys. E (Amsterdam, Neth.)* **2014**, *56*, 160.
- [41] Y. Jin, J. Wang, B. Sun, J. C. Blakesley, N. C. Greenham, *Nano Lett.* **2008**, *8*, 1649.
- [42] K. Keem, H. Kim, G.-T. Kim, J. S. Lee, B. Min, K. Cho, M.-Y. Sung, S. Kim, *Appl. Phys. Lett.* **2004**, *84*, 4376.
- [43] H. Kind, H. Yan, B. Messer, M. Law, P. Yang, *Adv. Mater.* **2002**, *14*, 158.
- [44] C. Baratto, E. Comini, G. Faglia, G. Sberveglieri, M. Zha, A. Zappettini, *Sens. Actuators B* **2005**, *109*, 2.
- [45] O. Lupan, G. Chai, L. Chow, *Microelectron. Eng.* **2008**, *85*, 2220.
- [46] A. Forleo, L. Francioso, S. Capone, P. Siciliano, P. Lommens, Z. Hens, *Sens. Actuators B* **2010**, *146*, 111.
- [47] E. Comini, *Anal. Chim. Acta* **2006**, *568*, 28.